Diffusion of Benzene and Propylene in MCM-22 Zeolite. A Molecular Dynamics Study

German Sastre,[†] C. Richard A. Catlow,[‡] and Avelino Corma*,[†]

Instituto de Tecnologia Quimica, U.P.V.-C.S.I.C., Universidad Politecnica de Valencia, Avenida Los Naranjos s/n, 46022 Valencia, Spain, and Davy Faraday Research Laboratory, The Royal Institution of Great Britain, 21 Albemarle Street, W1X 4BS London, U.K.

Received: December 17, 1998; In Final Form: March 3, 1999

Molecular dynamics simulations have been performed to study the diffusion of a mixture of benzene and propylene, for the cumene synthesis process, in purely siliceous MWW (MCM-22), a zeolite containing two separate channel systems: the 10-member ring (MR) sinusoidal and the 12-MR supercages interconnected by 10-MR windows system. The diffusion processes in each channel system of MWW at 650 K have been studied independently. We have found that in order to obtain quantitative or semiquantitative diffusion coefficients, the framework should be optimized. A large diffusivity for propylene in both channel systems, and especially in the supercage system, is observed, whereas benzene is not seen to diffuse in either of the two channel systems, and only intracage mobility is seen in the supercage voids. The positions of minimum energy, where the molecules are expected to react, have been located in both channels. The diffusion of benzene in the supercage system seems to be temperature-activated, and when the temperature is increased, intercage diffusion will probably occur. Radial distribution functions show that condensation reactions between benzene−propylene and propylene−propylene are possible, which indicate the necessity of working in an excess of benzene. The results of the simulations of diffusion suggest that the formation of cumene probably occurs at the external surface or close to the external surface of the MCM-22 zeolite crystals.

1. Introduction

The use of microporous materials for the alkylation of benzene with propylene to produce cumene (isopropylbenzene), a starting material for the production of acetone and phenol,[1] presents some advantages with respect to the mineral acids employed traditionally in this process. Thus, while $AlCl_3$, phosphoric acid, and others show good catalytic performance,[2,3] they raise environmental problems such as corrosion and waste disposal that are overcome by the use of microporous materials. In this respect technologies such as the DOW process[4] using Mordenite, the Mobil-Badger process[5] using H−ZSM-5, and CDTEC and ENI's process[6] using Y and β zeolites, respectively, unquestionably represent a progress.

Apart from environmental advantages, the use of zeolites presents the additional merit of reducing the amount of less desired products such as diisopropylbenzenes[7] but has the drawback of the formation of *n*-propylbenzene,[8] a product that is not formed in significant amounts when using mineral acid catalysts. It has been recently shown that *n*-propylbenzene is not formed, as originally thought, via monomolecular isomerization of the isopropyl isomer but rather from the transalkylation between propylbenzene and benzene.[9,10] In the case of zeolites, the pore dimensions and consequently the diffusion of the reactants and products are of paramount importance, since the final product distribution will depend highly on the zeolite channel structure. For instance, the formation of *n*-propyltoluene has been observed with ZSM-5[11] but not with Mordenite,[12] which suggests that the transalkylation reaction occurs in the 10-member ring (MR) channel intersections of ZSM-5, whereas the intersection of 12-MR and 8-MR channels in mordenite does not provide sufficient space for the bimolecular transalkylation process to occur. Following this line of argument, one could expect a higher yield of transalkylation in zeolite Y with respect to ZSM-5, which is, however, found to be much lower than in ZSM-5 under the same reaction conditions.[11] This experimental result indicates that the reactivity cannot be explained only in terms of the size of the cavities in which the reaction takes place, but the diffusion of the chemical compounds involved in the reaction also needs to be taken into account.

The mechanism for the alkylation of benzene with propylene occurs by first adsorbing the propylene on a Brønsted site, and then the resultant carbenium ion alkylates the benzene to give cumene.[13,14] Several zeolites such as H−ZSM-5, USY, β,[14] and MCM-22 have been tested for this reaction, and it has been found β, USY, and MCM-22 are very reactive. β zeolites with low Al content deactivate more rapidly, are less active, and produce more propylene oligomers, which seems to indicate that a low density of acid sites is beneficial for the catalyst decay/oligomerization of propylene. Another undesirable side reaction is the disproportionation of cumene with benzene, giving toluene and ethylbenzene, which only occur in large cavities.[7]

Zeolite MCM-22[15] (IZA code MWW), with a system of 10-MR pores and large 12-MR cavities connected by a single 10-MR window (see Figure 1), can show differences in the diffusion of benzene, propylene, and cumene, with corresponding implications for the location of the reaction. A previous study has looked into the diffusivity of cumene in the MWW structure,[16] where it has been found that there is a considerable activation energy for the process due to the larger relative size of the cumene molecule with respect to the 10-MR openings in the sinusoidal and the supercages system. Although the diffusion

* To whom correspondence should be sent.
[†] Universidad Politecnica de Valencia.
[‡] The Royal Institution of Great Britain.

10.1021/jp984776m CCC: $18.00
Published on Web 06/03/1999

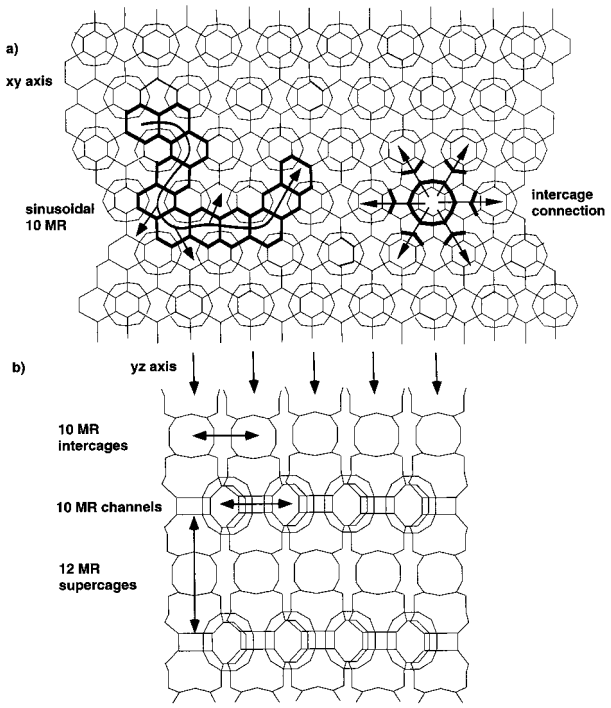

Figure 1. View of the independent void systems in MCM-22. (a) The sinusoidal 10-MR channels are all interconnected to each other and have a high degree of tortuosity. The large cavities contain six 10-MR windows interconnecting them. (b) The large cavities are 12-MR in cross-section size and are interconnected through short 10-MR conduits.

of cumene is shown to be more favorable in the supercages with respect to the 10-MR sinusoidal system, the 10-MR windows interconnecting the supercages still present a diffusion barrier for the cumene molecules. Reference 16 also compares the diffusion of cumene in the 10-MR channels of the MFI structure, where the diffusion is considerably larger because of the slightly larger size of the 10-MR channels in the MFI structure than in MWW, a point to which we return later.

The zeolite MCM-22 can be synthesized with framework Si/Al ratios below 150 using hexamethyleneimine as a template by following the original procedure reported in the patent literature,[15] or with Si/Al above that ratio up to the pure silica form (ITQ-1) using trimethyladamantammonium and hexamethyleneimine as structure-directing agents.[17] In the present work we are interested in investigating the diffusivity of benzene and propylene in each of the MCM-22 channels. As shown by our recent work,[18−20] molecular dynamics (MD) simulations offer a powerful way of probing molecular diffusivities in microporous materials. In this paper, therefore, the diffusion of benzene and propylene in ITQ-1 will be studied by MD techniques, leading to new insights into the factors controlling the cumene synthesis process.

2. Methodology

2.1. Molecular Dynamics Technique. Periodic atomistic molecular dynamics calculations have been performed to simulate the diffusion of a mixture of benzene and propylene in the purely siliceous MWW structure.[17] The simulation proceeds by first assigning initial velocities to all atoms according to a Maxwell−Boltzmann distribution that depends on the temperature of the system. From this starting point, Newton's equations of motion are solved using a finite time step by means of the standard Verlet algorithm.[21] The zeolitic system comprises a $2 \times 2 \times 2$ macrocell of SiO_2 composition with a total of 1728 atoms to which periodic boundary conditions are applied. The zeolite framework was first optimized at 0 K using the BFGS[22] technique implemented in the GULP[23] code, and the result is used as input for a 25 ps equilibration stage of the zeolite + sorbate system. After this period, runs of 200 ps, with a time step of 1 fs, were carried out within *NVE* microcanonical ensemble at 650 K. The temperature was equilibrated according to the Berendsen algorithm.[24] The loading simulated was eight molecules of benzene and eight molecules of propylene in the ITQ-1 macrocell, which corresponds to 1 molecule/unit cell for each hydrocarbon. Two separate runs were undertaken, one with the 16 molecules in the supercage system and the second with the 16 molecules in the 10-MR sinusoidal system.

In all the simulations, every atom was allowed to move explicitly. Although this increases substantially the computational expense, the influence of the framework flexibility has been made clear in a number of studies.[25−28] We have also performed additional calculations, keeping the zeolite framework fixed in order to study the influence of framework mobility on the hydrocarbon diffusivity.

The MD simulations have been carried out using the general purpose DL_POLY_2.0 code,[29] developed to run on parallel computers, written in the replicated data form and using standard message-passing libraries as well as highly optimized hardware specific communications. The code has been used on a CRAY-T3E MPP computer at the Edinburgh Parallel Computer Centre (EPCC). Most of the present simulations were run using 32 processors.

During the simulation, history files were saved every 200 steps, and subsequent analysis used the MSD facility included in DL_POLY to obtain mean-square displacements. The expression used to calculate the MSD plots was the following:[30]

$$\langle X^2(t)\rangle = \frac{1}{N_m N_{t_0}} \sum_m \sum_{t_0} [X_i(t+t_0) - (X_i(t_0)]^2 \qquad (1)$$

where N_m is the number of diffusing molecules, N_{t_0} is the number of time origins used in calculating the average, and X_i is the coordinate of the center of mass of molecule i.

The diffusion coefficients, D, are then calculated using the Einstein relation[30]

$$\langle X^2(t)\rangle = 6Dt + B \qquad (2)$$

where t is the simulation time and B is the thermal factor arising from atomic vibrations.

Also, as another analysis tool, the pair distribution functions, $g_{ab}(r)$, have been calculated from the history plots according to the expression[30]

$$g_{ab}(r) = \frac{1}{G_{ab}}[dN_{ab}/dV] \qquad (3)$$

where $N_{ab}(r)$ is the average number of a−b pairs with the distance between r and $r + dr$, G_{ab} is the density of "a" and "b" molecules, and V is the volume of the system.

The trajectories followed by the hydrocarbons in their diffusion path through the MWW structure are visualized by means of *xy* and *yz* projections, which highlight motion in the 10-MR sinusoidal channels and 12-MR supercage systems. The *trajectory graphs* contain all the visual information needed to understand, at first sight, the basic mechanism of the diffusion process; in particular, they allow us to see which molecules are diffusing through which channels. The *xy* projections are parallel

TABLE 1: Potential Form and Parameters Used for the Hydrocarbon Molecules

$V_{hydrocarbon} = V_{two-body} + V_{three-body} + V_{four-body} + V_{coul}$
$V_{two-body} = (1/2)k_{ij}(r_{ij} - r_{ij}^0)^2$
$V_{three-body} = (1/2)k_{ijk}(\theta_{ijk} - \theta_{ijk}^0)^2$
$V_{four-body} = A_{ijkl}[1 + \cos(n\phi_{ijk} - \delta_{ijkl})]$
$V_{coul} = q_i q_j / r_{ij}$
in benzene: $q(CB) = -0.153$; $q(HB) = +0.153$
in propylene: $q(C1) = -0.37$; $q(C2) = -0.12$; $q(C3) = -0.50$; $q(H) = +0.165$
(labeling as in $H_2-C1=C2H-C3H_3$)

two-body parameters	k_{ij} (eV Å^{-2})	r_{ij}^0 (Å)
CB−CB	48.94	1.385
CB−HB	31.25	1.085
C1−C2	60.59	1.335
C2−C3	27.46	1.520
C1−H	31.85	1.085
C2−H	28.71	1.095
C3−H	28.71	1.095

three-body parameters	k_{ijk} (eV)	q_{ijk}^0 (deg)
CB−CB−CB	3.44	120.0
CB−CB−HB	3.44	120.0
C1−C2−C3	6.87	121.5
C1−C2−H	4.06	121.0
C2−C1−H	4.06	121.0
C2−C3−H	2.50	109.5
C3−C2−H	6.87	117.5
H−C1−H	4.06	118.0
H−C3−H	2.06	109.2

four-body parameters	A_{ijkl} (eV)	n	δ_{ijkl} (deg)
CB−CB−CB−CB	0.2166	2.0	180.0
CB−CB−CB−HB	0.0867	2.0	180.0
HB−CB−CB−HB	0.0867	2.0	180.0
C1−C2−C3−H	−0.0087	3.0	0.0
C3−C2−C1−H	0.3254	2.0	180.0
H−C1−C2−H	0.3254	2.0	180.0
H−C2−C3−H	0.0108	3.0	0.0

to the 10-MR sinusoidal system, and the *yz* are parallel to the supercage system. To facilitate the visualization, the channel structure is superimposed over the trajectories of the center of mass. Also, *x* vs *t* graphs have been included to give an idea of the temporal evolution of the *x* coordinate of the center of mass.

We have also calculated the potential energy of the diffusing molecule along its trajectory, which allows comparison of the energy profiles of the different hydrocarbons as they diffuse through the different channels in the MWW structure. Finally, the activation energy of the benzene intercage crossing has also been calculated.

2.2. Interatomic Potentials. Four types of interatomic potentials are needed to model this system:

$$V_{total} = V_{zeolite} + V_{hydrocarbon} + V_{hc-hc} + V_{zeolite-hc} \quad (4)$$

The potential for the framework, $V_{zeolite}$, was originally derived by Catlow et al.[31] and is essentially a Born model potential comprising three-body interaction, short-range terms, and long-range Coulomb interaction. The potential for the sorbates, $V_{hydrocarbon}$, was taken from Oie et al.[32] and comprises two- (bond), three- (angle), and four-body (dihedral) interactions together with Coulomb terms. Two different atom types are considered in benzene, i.e., CB and HB, with a total of 12 bond terms, 18 angle terms, and 24 dihedral angle terms. Four different atom types were considered in propylene, i.e., C1, C2, C3, and H1, with a total of 8 bond terms, 12 angle terms, and 10 dihedral angle terms. All parameters used are given in Table 1.

Finally, 12−6 Lennard-Jones potentials, taken from Catlow et al.,[31] and Coulomb interactions were used to describe the hydrocarbon−hydrocarbon and framework−hydrocarbon interactions according to the following equations:

$$V_{hc-hc} = V_{Lennard-Jones} + V_{coul} \quad (5)$$

$$V_{zeolite-hc} = V_{Lennard-Jones} + V_{coul} \quad (6)$$

More details of the potential parameters[18] and the techniques employed can be found in previous studies.[19,20,33−36]

3. Results and Discussion

A schematic view of the channels of MCM-22 is shown in Figure 1. The interconnected sinusoidal channels are formed by 10-MR channels of dimensions 4.0 Å × 5.5 Å, and the independent 12-MR system is formed by large cages of 7.1 Å × 18.2 Å connected between them and with the external surface through 10-MR windows.

Two separate simulations have therefore been performed to explore independently the channel systems in the MCM-22 zeolite. The first contains 8 molecules of benzene and 8 molecules of propylene in the 12-supercage system, and the second contains the same number of hydrocarbon molecules placed in the 10-MR sinusoidal system. As the two channel systems in MCM-22 are independent, the separate treatment of each simulation allows us to make conclusions about the real structure, with the advantage of obtaining the information for each void system separately.

3.1. Flexible versus Frozen Framework. Diffusion Coefficients. The influence of framework flexibility has been reported to affect, in some cases, the diffusivity of the guest molecules, especially when the guest molecule matches the channel dimensions. The effect would be expected to be more pronounced for the more flexible structures. Such effects are apparent from the MSD plots obtained according to eq 1 and shown in Figure 2. The plots for benzene show that its diffusion is hindered in both channel systems, and a comparison of the flexible and frozen runs shows noticeable differences; interestingly, the diffusion is larger for the frozen framework. The larger diffusion of the smaller hydrocarbon, propylene, leads to extensive diffusion in both channel systems. Again, noticeable differences are expected when comparing flexible and frozen frames, the diffusion now being faster in the flexible frame. The diffusion coefficients, calculated according to eq 2, are shown in Table 2. We also note, in the case of propylene, a more linear plot in the case of the runs with the flexible framework, which further illustrates the advantages of optimizing the zeolite framework, when quantitative results on diffusion are required.

Besides allowing comparison between optimized and frozen MD simulations, the diffusion coefficients reported in Table 2 indicate a restricted diffusion of benzene in both the 10-MR and the supercage systems. On the other hand, diffusion of propylene is not restricted in either channel system with the diffusion through the supercage system being more than 10 times larger, behavior that we can rationalize from the trajectory plots.

3.2. Trajectories of Benzene and Propylene in the 10-MR Sinusoidal Channels. We recall that the system simulation by MD comprises a mixture of eight molecules of each hydrocarbon. Nevertheless, for the sake of clarity, the trajectory plots show the paths followed by each hydrocarbon separately. Figure 3 shows the trajectories followed by the benzene molecules, from which we clearly see that they are strongly impeded from

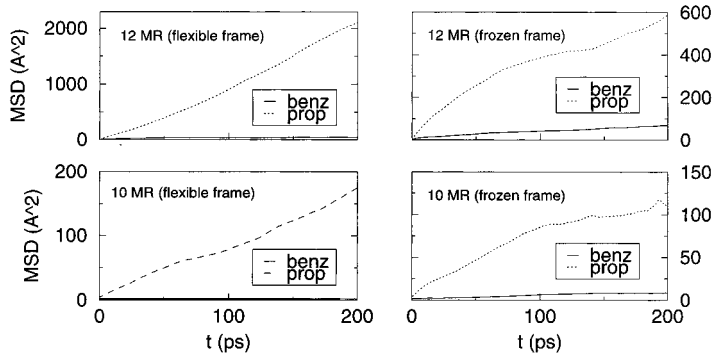

Figure 2. Mean-square displacements for the 200 ps runs of benzene + propylene diffusing in the sinusoidal system (10-MR) and the supercage system (12-MR) of MCM-22. The comparative results for the flexible and frozen frame show the influence of optimizing the framework. The diffusion coefficients for the optimized framework runs, obtained according to eq 2, are shown in Table 2.

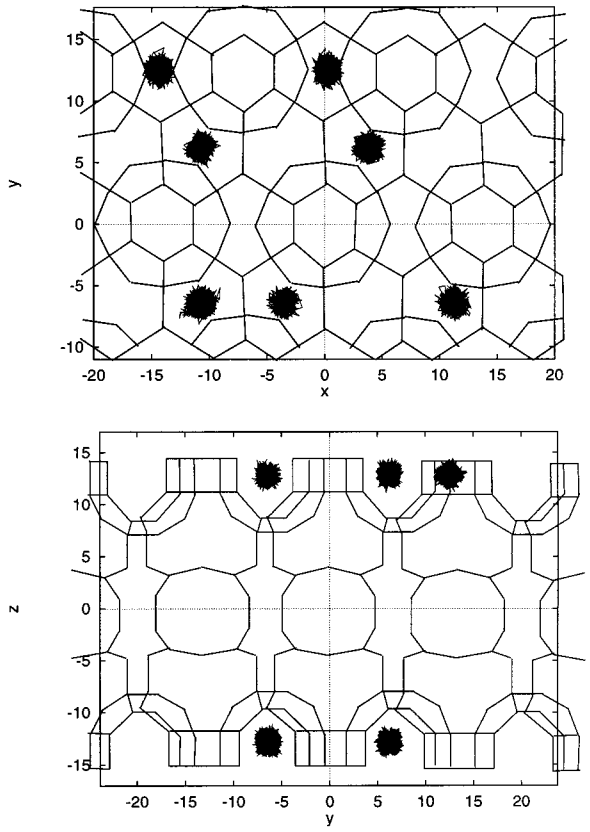

Figure 3. Trajectories of the eight benzene molecules diffusing through the 10-MR channels of MCM-22. It is seen that the molecules remain near their equilibrium positions, blocking partially the channels.

TABLE 2: Diffusion Coefficients Obtained from the Plots in Figure 2

	diffusion coefficients (cm^2/s)	
channel of diffusion	benzene	propylene
10-MR (flexible framework)		1.32×10^{-5}
10-MR (frozen framework)	6.60×10^{-7}	1.08×10^{-5}
12-MR (flexible framework)		1.79×10^{-4}
12-MR (frozen framework)	4.62×10^{-6}	4.11×10^{-5}

diffusing through the sinusoidal system, since they remain around their initial positions along the 200 ps run. Indeed, the trajectories of the centers of mass only move within a very restricted area around the minimun energy position. Although benzene molecules can normally diffuse through 10-MR channels, in the case of MCM-22 there is a high degree of tortuosity in the circular channel that will affect the mobility of this molecule. Moreover, the circular 10-MR channels in MCM-22 are smaller (4.0 Å × 5.5 Å) in size than those in ZSM-5 (5.3 Å × 5.6 Å and 5.1 Å × 5.5 Å for the straight and sinusoidal, respectively),[15,37] which would be expected to lead to a lower diffusivity of benzene in the sinusoidal system of MCM-22 compared with ZSM-5. Studies of benzene diffusivity followed by infrared techniques show that the diffusivity is slower in MCM-22 than in ZSM-5.[38,39] Such measurements give benzene diffusivities of 8.0×10^{-9} and 1.4×10^{-9} cm^2/s in ZSM-5 and MCM-22, respectively, at 400 K. Although these results cannot be quantitatively compared with our diffusion coefficients, we see that benzene diffuses more slowly in the 10-MR channels of MCM-22 than in those of ZSM-5, in line with the low diffusivity of benzene in the 10-MR channels of ITQ-1 found in our simulations.

A similar conclusion can be drawn from a recent computational study including the diffusion of cumene in MCM-22 and ZSM-5, where the activation energies have been calculated to be 90.0 and 18.6 kcal/mol in the sinusoidal channels of the MWW structure and in the channels of ZSM-5, respectively.[16] The present simulations showing the difficulty of diffusion of benzene through the 10-MR sinusoidal channels of MWW agree with the above results, although we do find appreciable mobility that could turn into a larger diffusivity at higher temperatures. Nevertheless, both the present and the previous results in ref 16 suggest strongly that the larger cumene molecules will not penetrate the MWW system and that most of the successful cumene production should occur either on or close to the external surface of the MWW structure.

The trajectories followed by the propylene molecules are shown in Figure 4, from which it can be seen that a much wider area is covered by these smaller molecules in their diffusion path through the 10-MR sinusoidal system. Careful inspection of Figure 4 shows that the trajectories are thiner in the channel intersections, indicating that the channel intersections correspond to locations of higher energy. This conclusion is in agreement with our previous results for benzene, where the minimum energy locations correspond to the nonintersecting parts of the sinusoidal channels. If the active centers for a given reaction are found in the nonintersecting parts of the 10-MR channel, then the reaction will be favored with respect to a competitive reaction, which can only occur at the crossing points of the 10-MR channels. Such behavior will be even more pronounced for benzene, and in this case, the reaction will not occur if the active centers were located at the channel intersections, although the effects of the temperature at which the reaction takes place could be critical, since the diffusion of the benzene through the sinusoidal system could be thermally activated and the reaction may then occur at higher temperatures.

3.3. Trajectories of Benzene and Propylene in the Super-

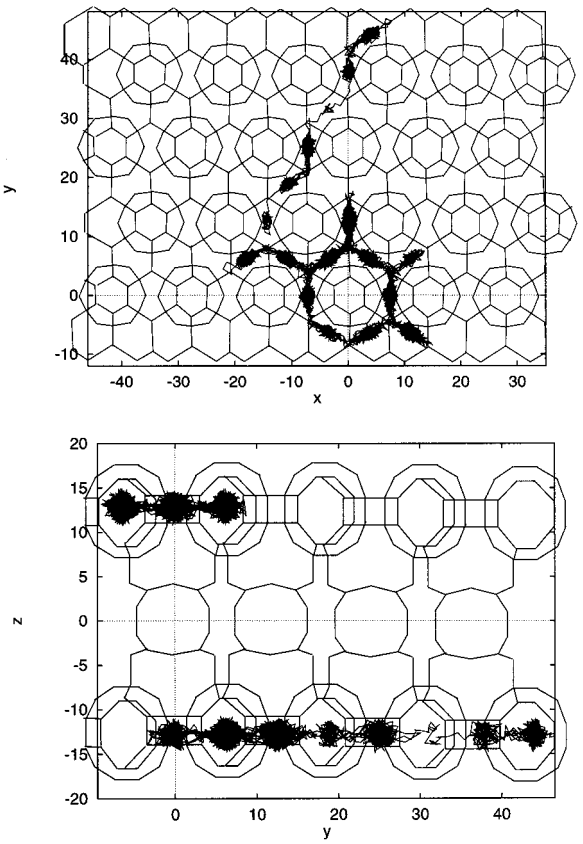

Figure 4. Trajectories of the eight propylene molecules diffusing through the 10-MR channels of MCM-22. It is seen that although part of the benzene molecules, not shown for clarity, are partially blocking the channels (see Figure 3), the propylene molecules can diffuse through the channels. The channel intersections correspond to the maximum energy positions as the molecules spend less time there.

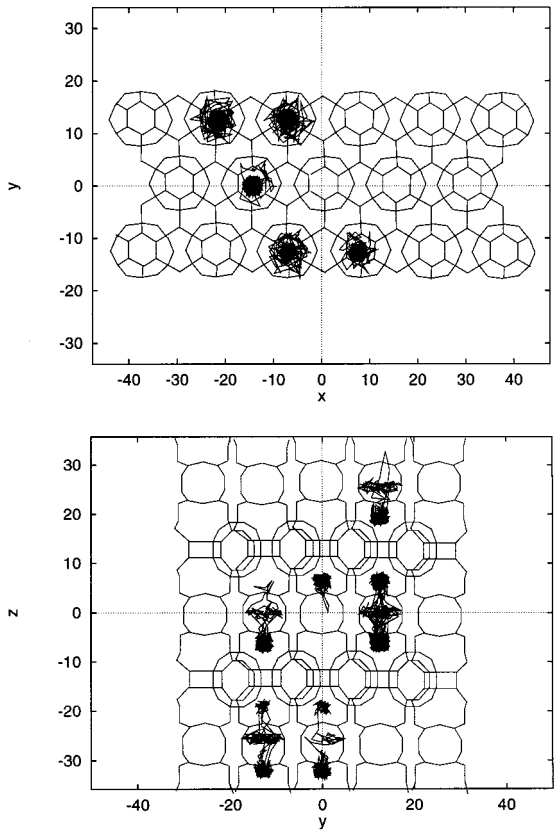

Figure 5. Trajectories of the eight benzene molecules diffusing through the supercages of MCM-22. Only intracage diffusion occurs, explaining the low diffusion coefficients obtained (Table 2), although some molecules spend a considerable time between the hemicages, near the crossing zone between cages, suggesting that increasing the temperature would activate the intercage diffusion.

cage System. The trajectories of benzene are shown in Figure 5, from which it can be seen that the molecules fill all the possible positions in one supercage. The *xy* projection indicates that the benzene molecules spend more time in the central part of the supercage, although there is also a considerable interaction with the walls of the cavity. The *yz* projection show two important features: the existence of two minimum energy positions at about the geometrical center of each hemicage and the intracage nature of the benzene motions. Each supercage is connected to another six supercages through 10-MR windows (Figure 1), and therefore, intercage motion is, in principle, possible. Nevertheless, migration of benzene molecules from one supercage to another has not been observed in this simulation, and this is in part due to the size and position of the 10-MR interconnecting windows, which are perpendicular to the direction of the motion (Figure 1). We consider that benzene intercage motions could be temperature-activated. In this respect, the *yz* trajectories (Figure 5) show a considerable time of residence in front of the 10-MR openings and very close to the crossing zone between supercages. The intracage diffusion observed for the benzene molecule explains the shape of the MSD plots observed in Figure 2 as the benzene molecules diffuse through a restricted part of the solid.

A completely different picture is found for the propylene molecules (Figure 6), where both graphs indicate a large diffusion path throughout the microporous structure with both intracage and intercage mobility observed. As in the case of benzene, the molecules of propylene spend most of the time inside the supercages, and crossing from one to another seems to require a certain activation energy, which indicates that in catalytic reactions, centers inside the supercages will be the most visited by the reacting molecules. Figure 7 shows the trajectory of an individual propylene molecule, which allows us to see in more detail the large part of the structure explored by a molecule in the 200 ps run.

From the results presented above one can envisage the synthesis of cumene in the supercage system as a process in which first the propylene molecules diffuse throughout the structure to find an active center, and as the whole structure is explored by the propylene molecule, one can imagine that propylene protonation will occur even when few active centers are available, independently of their location. Then the carbocation will diffuse until it finds a benzene molecule, which will occur at the hemicage positions where the benzene molecules spend most of their time. The resulting cumene molecules will remain for a period in the supercages, since their out-diffusion will become the controlling step and will be strongly dependent on temperature and loading. If any of the cumene molecules can diffuse out, this will better occur at low loadings when there are few propylene molecules obstructing the 10-MR openings, which are the only exits from the supercage system. In this hypothetical case it would thus be desirable to work at low propylene concentration, which is also favorable, since it minimizes the undesired propylene oligomerization and the formation of diisopropyl benzene. Nevertheless, it should be taken into account that if the cumene observed in the gas stream will mainly be formed in the large cavities, then the overall process will be controlled by the diffusion of cumene through the 10-MR windows, and then a lower reactivity should be observed. Then we propose that very little, if any, of

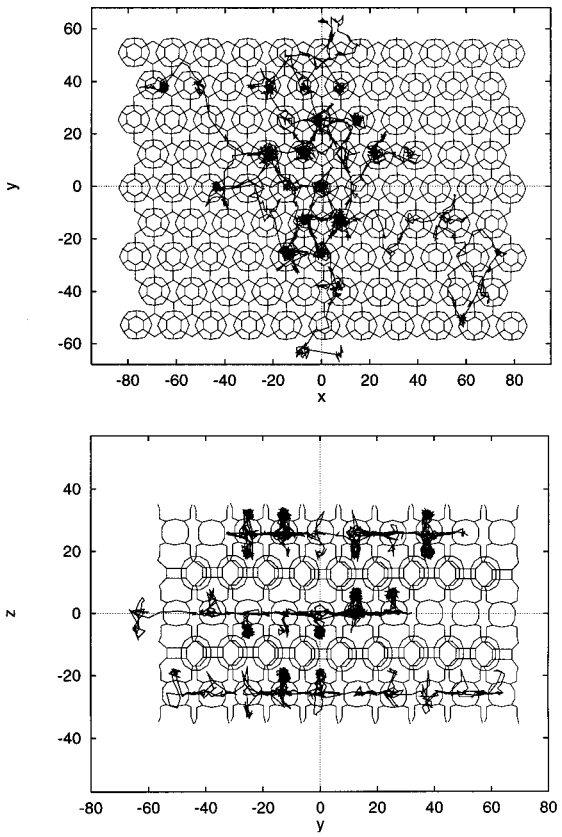

Figure 6. Trajectories of the eight propylene molecules diffusing through the supercages of MCM-22. The diffusion occurs both at the intracage and the intercage levels.

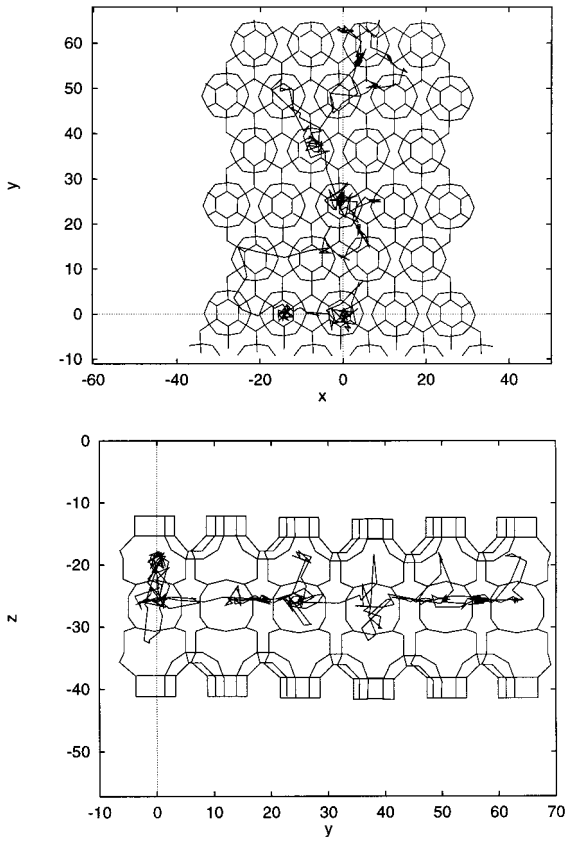

Figure 7. Trajectory of an individual propylene molecule from Figure 6, showing the large part of the microporous structure travelled by a single molecule.

the cumene produced during the alkylation on MCM-22 will be formed in the large cages but instead will form on the external surface at the end of the crystals.

3.4. Radial Distribution Functions. We have calculated the radial distribution functions, according to eq 3, to study the hydrocarbon−hydrocarbon intermolecular interactions. Figure 8 shows these interactions in the 10-MR sinusoidal channels. We note that the benzene molecules are relatively far from each other and that the number of pairs closer than 5 Å is very reduced. The other two possible pairs, propylene−benzene and propylene−propylene have very similar profiles, tending to lead to similar rates for benzene alkylation as for propylene oligomerization. Since cumene, if formed, will not be able to diffuse out of the 10-MR sinusoidal channels, our results predict that during the alkylation process the blockage of these channels will rapidly occur by formation of propylene oligomers as well as by some cumene molecule that will remain trapped into the system. Thus, one should not expect the 10-MR sinusoidal channels to intervene actively in the alkylation reaction.

Figure 9 shows the radial distribution functions corresponding to the hydrocarbons in the supercage system. The benzene−benzene plot in this case is governed by the fact that in one of the supercages there are two molecules of benzene, which is why the peaks near 3.75 and 6.5 Å are observed. The rest of the interactions would appear in the plot at distances larger than 10 Å. Apart from this isolated benzene−benzene interaction, we can say that benzene molecules are far from each other because at this temperature there is no intercage migration and cages are separated from each other by about 15 Å. The propylene−propylene interactions seem to be somewhat more important than benzene−propylene, which could be because of some partial blocking of the supercage entrances by benzene

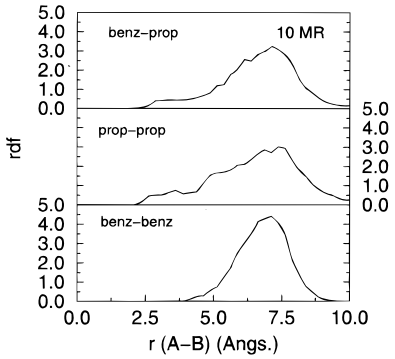

Figure 8. Radial distribution functions for hydrocarbon−hydrocarbon interactions inside the 10-MR sinusoidal channels of MCM-22.

molecules, which precludes the approach of the entering propylene molecule. Nevertheless, in both cases (propylene−propylene and benzene−propylene), the RDFs indicate the presence of two molecules in the same supercage, which will favor the reaction between them.

A comparison of the RDFs in the 10-MR sinusoidal channels (Figure 8) and the supercage system (Figure 9) reveals a slightly closer proximity for propylene−propylene and benzene−propylene in the supercage system compared to the 10-MR sinusoidal channels, which would indicate, as regards the channel structure, that there is a slightly better environment for cumene synthesis in the supercage system, although propylene oligomerization would also be more favorable there. Other variables, such as the level of loading and the location of the active centers, should also be studied in order to give a more complete picture of the relative rates of cumene synthesis in each void structure.

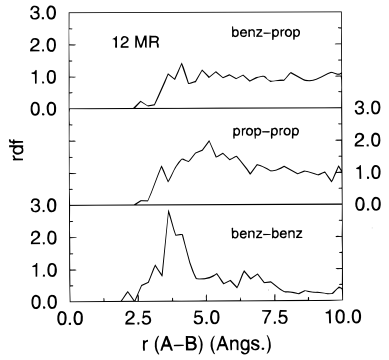

Figure 9. Radial distribution functions for hydrocarbon−hydrocarbon interactions inside the 12-MR supercage system of MCM-22.

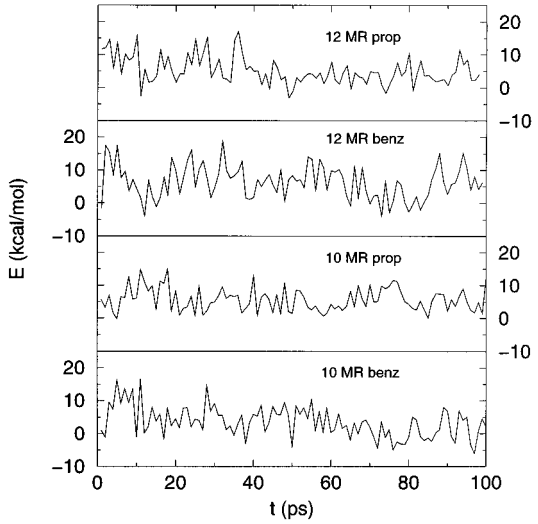

Figure 10. Diffusion energy profile of benzene and propylene in the 10-MR and 12-MR void systems of MCM-22.

3.5. Energetics of the Diffusion Process. The interaction energy between a single hydrocarbon molecule and the zeolite framework has been calculated from the MD trajectories. For the purpose we have taken the trajectory followed by a single molecule and we have calculated its energy according to

$$V_{\text{diffusion}} = V_{\text{hc(2-body)}} + V_{\text{hc(3-body)}} + V_{\text{hc(4-body)}} + V_{\text{zeo-hc(LJ)}} + V_{\text{zeo-hc(coul)}} \quad (7)$$

where the first three terms account for the conformational or internal energy of the hydrocarbon and where the fourth term corresponds to the Lennard-Jones interaction energy between the hydrocarbon and the zeolitic framework. The last term corresponds to the Coulomb interactions between the zeolite and hydrocarbon. We used the same potentials as in the MD simulations. The methodology for calculating these energy profiles is not implemented in the DL_POLY code, and the procedure followed was to obtain all the individual conformations for a 100 ps period (a total of 400 conformations, since they were saved every 0.25 ps) and to calculate the interaction energy using the general purpose static lattice simulation feature available in the GULP program[23] with the energy being evaluated using eq 7 in a single-point calculation for every conformation.

The results are evaluated for a single benzene or propylene molecule diffusing inside the supercage and the sinusoidal systems. Figure 10 shows that all the energy profiles are somewhat similar, with maxima in the interaction energy of around 15−20 kcal/mol and minima about −5 kcal/mol, which

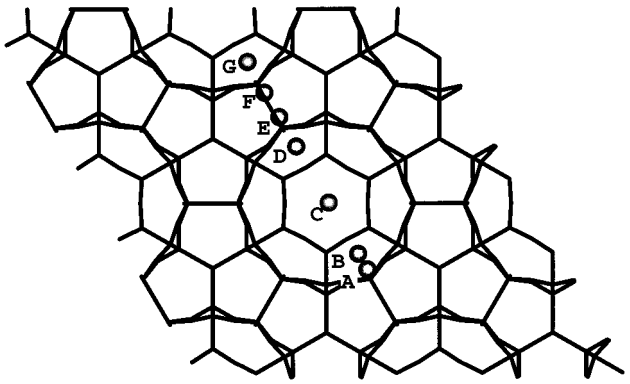

Figure 11. Top view of the MCM-22 structure showing the trajectory and the critical points (A−F) followed by benzene as it is pulled from cage to cage.

shows the energy available for diffusion of benzene and propylene at 650 K. Any process requiring an activation energy higher than 20 kcal/mol would not be observed at this temperature. Obviously, the different nature and size of each molecule allows them to explore different parts of the solid. For instance, the trajectory graphs show that benzene cannot cross from one part of the 10-MR channel to the other (Figure 3) with that energy, whereas the available thermal energies are sufficient for the propylene to diffuse through the 10-MR channels (Figure 4). A similar conclusion is drawn when inspecting the energy profiles of the diffusion through the supercages (Figure 10). Benzene molecules remain inside the cavities with insufficient energy to overcome the crossing barrier, whereas in the case of propylene thermal energies are sufficient for the molecules to diffuse throughout the entire supercage system.

3.6. Activation Energy of Benzene through the 10-MR Interconnecting Cages. To obtain a more clear picture of the benzene intercage motion, an event not observed in our MD runs, we have to employ a different technique. For this purpose we have forced a single benzene molecule to follow the path connecting two supercages in the MWW structure. First, we have used a simple docking strategy with the Discover software[40] to optimize the conformation of the benzene molecule as it crosses from cage to cage. Second, we have divided the corresponding path into small steps 0.25 Å distant from each other, and for all the corresponding conformations, we have calculated the interaction energy between the benzene and the zeolite framework with the GULP code, in a similar way as explained in the above paragraph, and used the force field shown in eq 7. The benzene is thus pulled through the trajectory showed in Figures 11 and 12. Furthermore, we have considered two different orientations for the benzene molecule in crossing from cage to cage, as shown in Figure 12. The energy profiles calculated by this technique are shown in Figure 13. Orientation-2 (Figure 13, bottom) shows a higher activation energy and does not correspond to the path expected to be followed in an intercage jump. Orientation-1 shows a more favorable energetic profile, and for this case, we have calculated the separate contributions to the activation energy. The first contribution comes from the first four terms in eq 7, and that is the Lennard-Jones plus the benzene conformational energy. The second contribution comes from the electrostatic interaction between the benzene and the zeolite structure. As Figure 13 (middle graphic) shows, both contributions are important, and the total energy profile is then shown in the top graphic (Figure 13). The points highlighted as E and F correspond to the intercage space (Figures 11 and 12), and they are the points of maximum

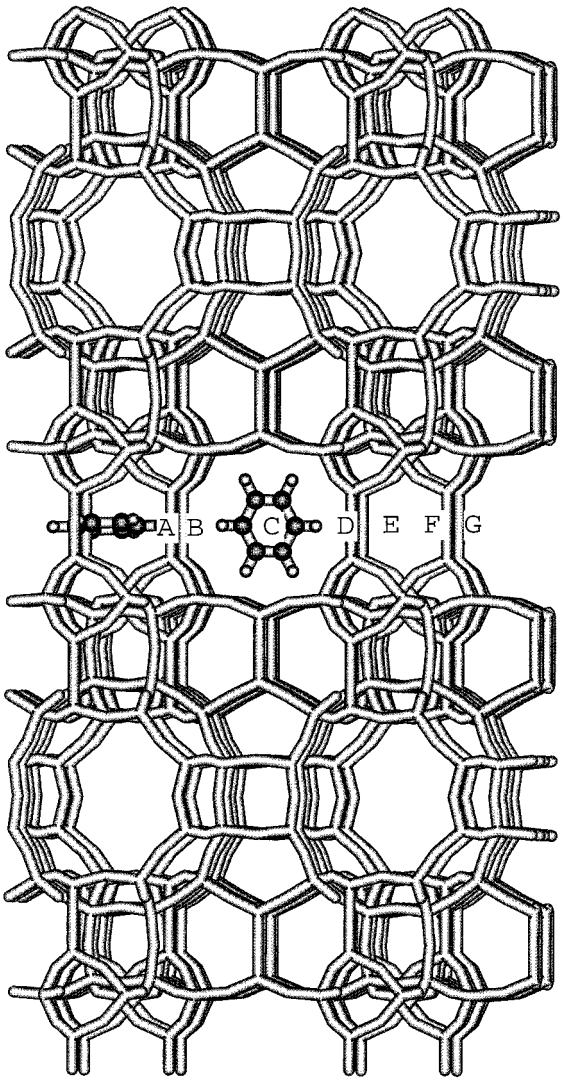

Figure 12. Side view of the MCM-22 structure showing the trajectory and the critical points (A−F) followed by benzene as it is pulled from cage to cage.

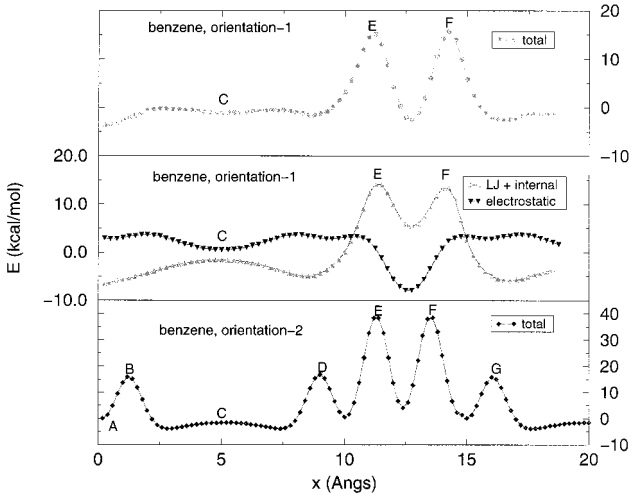

Figure 13. Energy profile of benzene as it is pulled from cage to cage in the MCM-22 structure following the trajectories shown in Figures 11 and 12. Two energy paths have been tried, with orientation-1 (left benzene in Figure 12) and orientation-2 (right benzene in Figure 12). Orientation-2 (bottom graph) gives a higher activation energy, and thus, orientation-1 is preferred. For the latter, the two energy components (electrostatic and Lennard-Jones plus benzene internal energy) are plotted in the middle graph and the total energy is shown in the top graph. The interaction energy between benzene and zeolite has been calculated according to eq 7.

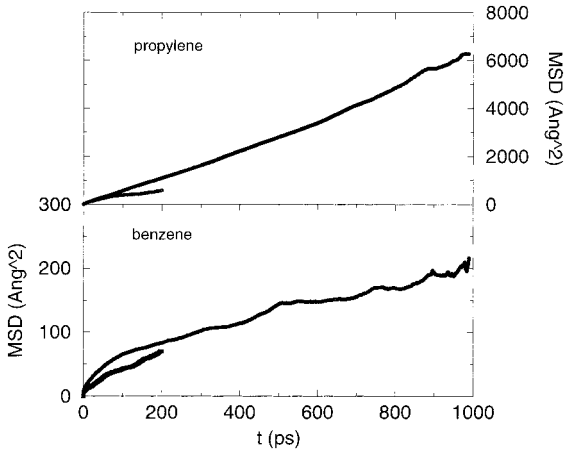

Figure 14. Mean-square displacements for the 1000 ps run of benzene + propylene diffusing in the supercage system (12-MR) of MCM-22 at 850 K. This run has been performed with a rigid zeolite framework. The MSD plots for the previous simulation with a rigid framework at 650 K are also shown for the sake of comparison.

energy. The energy necessary to cross from cage to cage is around 15 kcal/mol (Figure 13, top), and the previous results from Figure 10 show that this is still in the range of the thermal energy of the benzene molecules. Nevertheless, apart from the fact that the energy of the benzene molecules is just about what is needed to cross from cage to cage, we have seen that if the orientation of the benzene molecule is not adequate with respect to the 10-MR window, the benzene molecule is rejected from the intercrossing region as a consequence of the energetic profile becoming higher in energy, as in the bottom graph in Figure 13. This allows us to conclude that occasionally some benzene molecules can cross from one cage to another and that increasing the temperature would possibly increase the probability of observing benzene intercage motions. The presence of other sorbate molecules can influence the calculated activation energy through the sorbate−sorbate interactions not taken into account in these calculations.

3.7. Diffusion of Benzene through the Supercage System at 850 K. To test whether the intercage diffusion of benzene is an activated process, we have performed an additional simulation at 850 K. The same loading that was used in the preceding simulations has been employed in this case. We have extended the simulation over a longer period, 1000 ps, to obtain a more realistic picture of the process. The simulations have been carried out with a fixed framework in order to save computer time. The total run has been carried out using 16 processors and has taken 640 h on a CRAY-T3E. The MSD plots are shown in Figure 14, and it can be seen that the plot for the case of benzene is not very linear, thus indicating that the diffusion coefficient cannot be estimated with precision by this technique, since the sorbate is not diffusing throughout the whole zeolite crystal. For the case of propylene, the MSD plot is linear because of its higher diffusivity through the structure and a diffusion coefficient of 1.05×10^{-4} cm^2/s is obtained. This is larger than that obtained from the corresponding 200 ps simulation (frozen framework) by a factor of 2.5. The two MSD plots are drawn in Figure 14 to make the differences more visible. For the purpose of this simulation we have focused our attention on the trajectories of the benzene molecules (Figure 15). We note that, as in the previous case at 650 K, the benzene molecules spend most of their time inside the supercage system as was

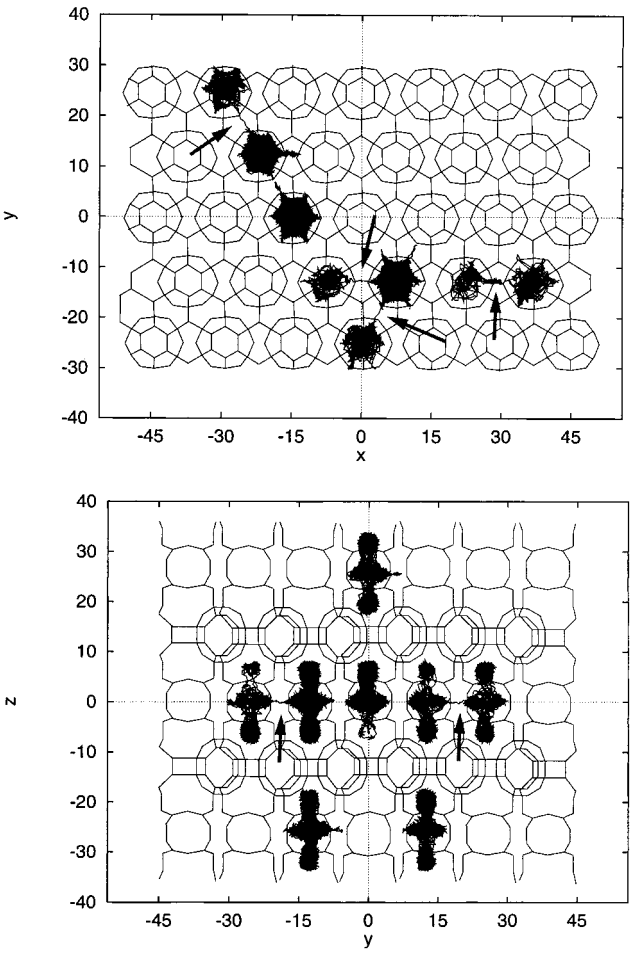

Figure 15. Trajectories of the eight benzene molecules diffusing through the supercage system of MCM-22. The graphic corresponds to the 1000 ps simulation at 850 K. The eight propylene molecules, also included in the simulation, are not shown for clarity. Intercage migration is observed at this temperature, and the four events (only two are visible in the *yz* projection) are highlighted with arrows.

expected. However, in the present case, some intercage crossing events have been found. There are only four such events in the 1000 ps run, but they suffice to show the possibility of this motion and its temperature-activated nature. It is also seen that the intercage motions are infrequent and that they take place on a different scale of time than the intracage diffusion. In real systems, where longer relaxation times are used to measure diffusivity, both intracage and intercage diffusion of benzene in MCM-22 should be observed if the temperature is high enough to activate the process.

4. Conclusions

Periodic atomistic molecular dynamics simulations have been performed to simulate the diffusion of a mixture of benzene and propylene in a purely siliceous MWW structure. Two separate simulations have been carried out to explore independently diffusion processes in each channel system of the MWW at 650 K. The diffusing mixture of benzene and propylene corresponds to the synthesis of cumene, and the behavior of the reactants in each channel allows us to understand better the diffusional aspects of the synthesis. From the methodological viewpoint, the necessity of optimizing the framework in order to obtain quantitative or semiquantitative diffusion coefficients has been proved. It is seen from the mean-square displacement (MSD) plots that benzene shows low diffusivity in both of the two pore systems, which is due to the small size of the 10-MR openings of the sinusoidal system and to the location of the 10-MR windows in the supercages that are perpendicular to the direction of the motion. On the other hand, the MSD plots also show a large diffusivity for propylene in both channel systems and especially in the supercage system, and we are able to calculate the independent diffusion coefficients in each channel, which would be difficult to obtain from experiments. The trajectory analysis for benzene shows little motion around the energy minima in the 10-MR sinusoidal channels and an intracage diffusion in the supercage system. In the case of propylene, the diffusion occurs throughout both channels in all their extension. The positions of minimum and maximum energy have been located in both channels, and the molecules are expected to react close to the minimum energy locations, provided the acid centers are located nearby. The diffusion of benzene in both the sinusoidal and the supercage systems seems to be thermally activated, and increasing the temperature would probably allow higher mobilities in both cases. We have calculated the activation energy of benzene in the intercage migration process, and we have found that at the simulation temperature the thermal energy allows the mobility of benzene inside the cavity but not the crossing from one cavity to another, a process for which a higher temperature and/or much longer simulations would be required. An additional and longer simulation at 850 K shows that this is the case, and some intercage diffusion events are found for the benzene molecules. In the case of the 10-MR sinusoidal channels, the low diffusivity of benzene may be surprising if compared with other 10-MR zeolites, which we explain by the relatively small size of the 10-MR channels in the MWW structure and by its high degree of tortuosity.

The radial distribution functions show that condensation reactions between benzene−propylene and propylene−propylene are possible and perhaps more probable in the supercage system. Both reactions seem favorable with a larger possibility for propylene oligomerization. The present work suggests that owing to the relative size of benzene−cumene and pore diameter, most of the successful reactions will occur at the external surface or close to the external surface.

Acknowledgment. G.S. thanks Ministerio de Educacion y Ciencia of Spain for a research contract to work at the ITQ in Valencia and the CICYT Project MAT-97-1016-C02-01 for financial support. We thank Dr. W. Smith for useful discussions regarding DL_POLY code. The EPCC (Edinburgh Parallel Computer Centre) and the EPSRC funded CRAY-T3E Materials Chemistry Consortium are gratefully acknowledged.

References and Notes

(1) Pujado, P. R.; Salazar, J. R.; Berger, C. V. *Hydrocarbon Process.* **1976**, *55*, 91.

(2) Miki, H. U.S. Patent, 4347393, 1982.

(3) Jones, E. K.; Dettner, D. D. U.S. Patent, 2860, 1958.

(4) Wood, A. *Chem*. Week **1994**, August 17, 34.

(5) Kaeding, W. W.; Holland, R. E. *J. Catal.* **1988**, *19*, 212.

(6) Chen, J. Presented at Worldwide Solid Acid Process Conference, Houston, TX, November 14−16, 1993.

(7) Medina-Valtierra, J.; Zaldivar, O.; Sanchez, M. A.; Montoya, J. A.; Navarrete, J.; de los Reyes, J. A. *Appl. Catal. A* **1998**, *166*, 387.

(8) Chandavar, K. H.; Hedge, S. G.; Kulkarni, S. B.; Ratnasamy, P. *J. Chem. Technol. Biotechnol*. **1984**, *34A*, 165.

(9) Ivanova, I. I.; Brunel, D.; Nagy, J. B.; Daelen, G.; Derouane, E. G. *Stud. Surf. Sci. Catal.* **1993**, *78*, 587.

(10) Wichterlova, B.; Cejka, J. *J. Catal.* **1994**, *136*, 523.

(11) Cejka, J.; Kapustin, G. A.; Wichterlova, B. *Appl. Catal.* A **1994**, *108*, 187.

(12) Wichterlova, B.; Cejka, J.; Zilkova, N. *Microporous Mater*. **1996**, *6*, 405.
(13) Geatti, A.; Lenarda, M.; Storaro, L.; Ganzerla, R.; Perissinotto, M. *J. Mol. Catal. A* **1997**, *121*, 111.
(14) Bellusi, G.; Pazzuconi, G.; Perego, C.; Girotti, G.; Terzoni, G. *J. Catal*. **1995**, *157*, 227.
(15) Leonowicz, M. E.; Lawton, J. A.; Lawton, S. L.; Rubin, M. K. *Science* **1994**, *264*, 1910.
(16) Perego, C.; Amarilli, S.; Millini, R.; Bellusi, G.; Girotti, G.; Terzoni, G. *Microporous Mater*. **1996**, *6*, 395.
(17) Camblor, M. A.; Corell, C.; Corma, A.; Diaz-Cabañas, M. J.; Nicopoulos, S.; Gonzalez-Calbet, J. M.; Vallet-Regi, M. *Chem. Mater*. **1996**, *8*, 2415.
(18) Sastre, G.; Raj, N.; Catlow, C. R. A.; Roque-Malherbe, R.; Corma, A. *J. Phys. Chem. B* **1998**, *102*, 3198.
(19) Corma, A.; Catlow, C. R. A.; Sastre, G. *J. Phys. Chem. B* **1998**, *102*, 7085.
(20) Sastre, G.; Corma, A.; Catlow, C. R. A. *Top. Catal*., in press.
(21) Verlet, L. *Phys. Rev.* **1967**, *159*, 98.
(22) Shannon, D. F. *Math. Comput*. **1970**, *24*, 647.
(23) Gale, J. D. *J. Chem. Soc., Faraday Trans*. **1997**, *93*, 629.
(24) Berendsen, H. J. C.; Postma, J. P. M.; van Gunsteren, W.; DiNola, A.; Haak, J. R. *J. Chem. Phys*. **1984**, *81*, 3684.
(25) Deem, M. W.; Newsam, J. M.; Creighton, J. A. *J. Am. Chem. Soc*. **1992**, *114*, 7198.
(26) Demontis, P.; Fois, E. S.; Suffriti, G. B.; Quartieri, S. *J. Phys. Chem.* **1990**, *94*, 4329.
(27) Yashonat, S.; Thomas, J. M.; Nowak, A. K.; Cheetham, A. K. *Nature* **1988**, *331*, 601.
(28) Schrimpf, G.; Schlenkrich, M.; Brickmann, J.; Bopp, P. *J. Phys. Chem.* **1992**, *96*, 7404.
(29) Smith, W.; Forester, T. R. *J. Mol. Graphics* **1996**, *14*, 136.
(30) Allen, M. P.; Tildesley, D. *Molecular Simulation of Liquids*; Oxford University Press: Oxford, U.K., 1980.
(31) Catlow, C. R. A.; Freeman, C. M.; Vessal, B.; Tomlinson, S. M.; Leslie, M. *J. Chem. Soc., Faraday Trans*. **1991**, *87*, 1947.
(32) Oie, T.; Maggiora, T. M.; Christoffersen, R. E.; Duchamp, D. J. *Int. J. Quantum Chem., Quantum Biol. Symp*. **1981**, *8*, 1.
(33) Klein, H.; Fuess, H.; Schrimpf, G. *J. Phys. Chem.* **1996**, *100*, 11101.
(34) Nicholas, J. B.; Trouw, F. R.; Mertz, J. E.; Iton, L. E.; Hopfinger, A. J. *J. Phys. Chem*. **1993**, *97*, 4149.
(35) Hernandez, E. Ph.D. Thesis, University College, London, 1993.
(36) Auerbach, S. M.; Henson, N. J.; Cheetham, A. K.; Metiu, H. I. *J. Phys. Chem*. **1995**, *99*, 10600.
(37) Meier, W. M.; Olson, D. H.; Baerlocher, Ch. *Atlas of Zeolite Structure Types*, 4th ed.; Elsevier: Amsterdam, 1996.
(38) Roque-Malherbe, R.; Wendelbo, R.; Mifsud, A.; Corma, A. *J. Phys. Chem.* **1995**, *99*, 14064.
(39) Corma, A. *Microporous Mesoporous Mater*. **1998**, *21*, 487.
(40) *Discover*; Molecular Simulations Inc., 1998.